Analysis of Gain in Determining T_0 in 1.3 μm Semiconductor Lasers

David A. Ackerman, Gleb E. Shtengel, Mark S. Hybertsen, Paul A. Morton, *Member, IEEE*, Rudolf F. Kazarinov, T. Tanbun-Ek, and R. A. Logan

Abstract— **Rapid decrease of differential gain has been determined to dominate the temperature dependence of threshold current in 1.3-μm multiquantum well and bulk active lasers giving rise to low values of T_0. Extensive experimental characterization of each type of device is described. Results are presented for the dependence of gain on chemical potential and carrier density as a function of temperature. The data indicate the important role of the temperature-insensitive, carrier density dependent chemical potential in determining differential gain. Modeling of the temperature dependence of threshold carrier density in MQW and bulk active lasers based on a detailed band theory calculation is described. The calculated value of T_0 depends on the structure of the active layer, e.g., multiquantum well versus bulk. However, the calculated values are substantially higher than measured.**

I. Introduction

WIDESPREAD use of low cost 1.3-μm broad-band fiber-optic links is forecast for the near future. Low cost semiconductor laser modules are favored for these systems which must operate over a wide temperature range without the aid and added expense of thermoelectric cooling elements. Lasers for such applications must therefore possess reasonably uniform operating characteristics between temperatures of -40 and 85 °C. Temperature dependence in semiconductor lasers is frequently characterized by the empirical parameter T_0 [1]. Unfortunately, long wavelength InGaAsP–InP based semiconductor lasers are well known to exhibit strong temperature dependence of threshold over this temperature range (low T_0) compared to shorter wavelength GaAs based lasers. The aim of this study is to examine the temperature dependence of 1.3-μm semiconductor lasers in an attempt to identify a mechanism underlying this troublesome threshold temperature dependence.

Temperature dependent optical loss [2]–[4] as well as heterobarrier leakage [5] have been cited as the main cause of observed temperature sensitivity of threshold. Many prior investigations have indicated nonradiative recombination due to various Auger processes as the primary cause of strong threshold temperature dependence in long wavelength lasers [6]–[15]. Most of the studies of Auger recombination have focused on either the temperature dependence of the Auger processes [8], [11], [13], [15] or the role of Auger processes in consuming current [6], [7], [9], [10], [12], [14]. While there is no consensus on the temperature dependence, it is generally agreed that the non-linear dependence of Auger recombination on carrier density tends to boost long wavelength laser thresholds with temperature. Recently however, in contrast to previous findings [16], [17], gain has been identified as a dominant cause of poor (low) T_0 in 1.55-μm strained MQW lasers [18], 1.3-μm strained multiquantum well (MQW) and bulk lasers [19], [20], and 0.98-μm Al-free strained single- and multiquantum well lasers [21].

In this study, we present extensive experimental characterization of 1.3-μm multiquantum well and bulk active lasers including measurements of gain, loss and chemical potential as a function of injected carrier density and temperature. We focus on carrier density rather than current as an independent variable. In so doing, we avoid the need to analyze the temperature dependence of recombination processes. On the basis of our experimental findings, we confirm that the temperature dependence of differential gain dominates the temperature dependence of threshold carrier density and threshold current in the lasers studied. Data are presented in terms of gain as a function of chemical potential, carrier density and temperature. Predictions of a gain model based on an accurate band structure are presented and compared to experiments in Section III, followed by conclusions of this study.

II. Experimental

A. Devices

Devices used in this study consisted of MQW and bulk active 1.3-μm capped mesa buried heterostructure [22] (CMBH) Fabry–Perot lasers that are designed for use in uncooled laser modules. Multiquantum-well lasers contained from 7 to 10 wells of strained quaternary material with quaternary barriers of thickness ~100 Å. Well thicknesses ranged from 30 to 100 Å with compressive strain between 0.3 and 1.0%. Bulk lasers contained 1300-Å thick unstrained quaternary active regions. Laser cavities of ~1 μm width and ~300 μm length were surrounded by conventional InP current blocking layers. Chips with uncoated facets were bonded with the substrate-side down on ceramic heatsinks.

Lasers of the type described above exhibit low current leakage. Leakage is characterized by measurement of differential impedance above threshold. A drop in differential impedance dV/dI is an indication of leakage arising from either shunt paths around the active layer or heterobarrier leakage at the active-cladding interface [23]. With low leakage, internal efficiency η_{int} remains high (~80%) over the operating tem-

Manuscript received October 20, 1994; revised January 18, 1995.
The authors are with AT&T Bell Laboratories, Murray Hill, NJ 07974 USA.
IEEE Log Number 9411685.

1077–260X/95$04.00 © 1995 IEEE

perature range as will be discussed. Typical external slope efficiencies at 25 °C were measured to be 0.24 W/A/facet, dropping to 0.20 W/A at 85 °C. CMBH lasers of the present design typically exhibit 3-dB parasitic-limited bandwidths of 10 to 12 GHz at operating powers of ~10 mW.

B. Measurement Techniques

Amplified spontaneous emission (ASE) spectra were measured for each laser between 25 and 85 °C for a series of closely spaced sub-threshold bias currents. An HP-70951A optical spectrum analyzer with 0.1 nm resolution was used. A polarizer with extinction ratio ~40 dB incorporated between laser facet and spectrometer allowed selection of either TE or TM polarized spontaneous emission from the laser. Modal gain was determined by analyzing the spectral fringe contrast of ASE [24], [25]. In our case, the ratio of longitudinal mode spacing to spectrometer resolution was approximately 10. We found that the prescription of [25] gave more accurate gain results than the often used formulation of [24] for net gains in excess of ~ -30 cm^{-1}. Error of measurement of modal gain determined in this fashion was found to be ± 0.5 cm^{-1} over almost the entire energy range. Accuracy of gain measurement on the low-energy side of the gainpeak was limited by the level of stray light rejection in our spectrometer of ~ -60 dB.

Loss was determined in each laser as a function of sub-threshold current and temperature using a technique which represents a variation of that described in [26] and which will be reported upon elsewhere [27]. A small, single-frequency, ac optical signal from a HP-8167A external cavity laser was introduced into a laser cavity. The induced ac voltage response across the laser under test was monitored while sweeping the photon energy of the external source. Resulting detection curves show peaks corresponding to cavity resonances of the laser under test. The envelope of these peaks is approximately proportional to material gain. Under conditions of transparency, at which point material gain switches sign, the envelope of the peaks also passes through zero. Location of the photon energy corresponding to this zero gives an accurate means of determining transparency energy which was then recorded at each current and temperature. We find this method of identifying material transparency superior to others due to its immunity to effects of out-of-band optical emission from the external source.

Residual loss in the laser cavity at the determined transparency energy was obtained using the spectral fringe contrast method described above. Loss measured under conditions of material transparency is ascribed to free carrier and intervalence band absorption, absorption due to modal overlap with doped cladding material and a small amount of scattering, all lumped together as α_{int}, and to mirror loss α_m. Due to the extremely strong dependence of material loss (or gain) on photon energy in the neighborhood of transparency (approximately 5 cm^{-1}/meV), it is essential to measure transparency energy accurately. In our measurements, error in loss at transparency of less than ± 1 cm^{-1} implied an error of measurement of transparency energy of better than ± 0.2 meV (± 0.25 nm) or better.

Comparison of the peak modal gain to loss at transparency, provides a measure of the maximum net modal gain available at a given current and temperature. In subtracting peak gain from loss at the transparency energy, we neglect the small variation in loss which occurs over this small energy range. Estimating variation in free carrier absoprtion and intervalence band absorption [28], a roughly constant, small error in net gain of ~ 1 cm^{-1} is incurred.

Differential carrier lifetime τ_d was determined as a function of sub-threshold current and temperature by first measuring the sub-threshold frequency response of spontaneous emission collected from a laser facet under small-signal electrical modulation [29]. Samples selected for this study showed clean, parasitic-free roll-off characteristics which could be well fit by a single pole (i.e., a single time constant τ_{sp}) between 1 and 1000 MHz. The values for τ_{sp} are then corrected, taking into account the measured bias-dependent differential junction impedance $R_d/(1+i\omega\tau_d)$ in series with the source impedance (50 Ω) and laser series impedance [30].

Internal efficiency η_{int} was estimated for each device by comparing total external slope efficiency at threshold $L'(I_{\text{th}})$ to the ratio of mirror to total loss, also at threshold using the relationship $L'(I_{\text{th}}) = (1.24/\lambda[\mu\text{m}]) \cdot \eta_{\text{int}} \cdot \alpha_m/\alpha_{\text{total}}$.

C. Experimental Results and Analysis

Representative gain spectra for a multi-quantum well laser are illustrated in Fig. 1(a), in which modal gain is plotted as a function of photon energy for various subthreshold laser drive currents at a fixed temperature of 25 °C. At low energy, the spectra converge to approximately -60 to -70 cm^{-1}, a value close to total loss measured at transparency. Measured loss at material transparency energy is also plotted in Fig. 1(a) (diamonds) for each current. At threshold, measured modal gain is zero to within our experimental accuracy of ± 0.5 cm^{-1}. Gain spectra for a bulk active laser, such as those shown in Fig. 1(b) are qualitatively similar to spectra obtained for MQW lasers, although broader by about 10 meV. Gain spectra for MQW and bulk active lasers at 85 °C are shown in Fig. 2(a) and (b), respectively. In both MQW and bulk active cases, we see a broadening of spectra with temperature. Between 25 and 85 °C, the rate of broadening with carrier density is observed to be roughly linear as shown in Fig. 3. The slope of modal gain peak width (full spectral width at half peak net gain) as a function of carrier density for the bulk case in Fig. 3 is reduced slightly from 25 to 85 °C, dropping approximately 30% from 25 to 18 meV/10^{18} cm^{-3}. In the MQW case, this slope remains constant to within ~10% at 8 meV/10^{18} cm^{-3}.

Differential lifetime as a function of bias current and temperature is plotted in Fig. 4(a) and (b) for MQW and bulk active lasers. Carrier density was then determined by integrating τ_d over current [31] taking account of internal efficiency. Resulting current as a function of carrier density is plotted in Fig. 5(a) and (b) for the same MQW and bulk active lasers featured in Figs. 1 and 2. A strong temperature dependence in the relationship of current versus carrier density was not observed. Our results, which are in accord with those of Zou *et al.* [18], hold for both MQW and bulk active lasers. Results

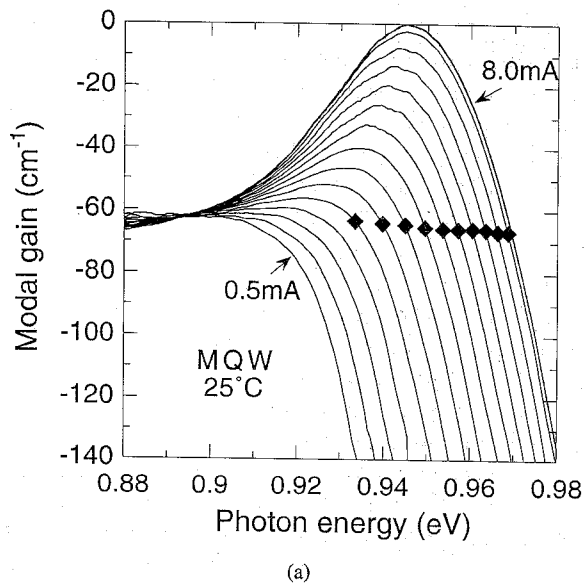

(a)

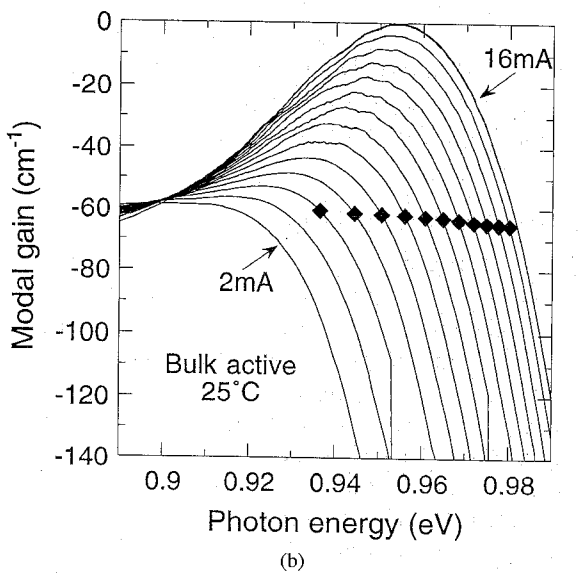

(b)

Fig. 1. Sub-threshold, 25 °C modal gain spectra as a function of photon energy for (a) MQW laser for various currents (in 0.5 mA current steps) and (b) bulk active laser (1 mA current steps). Diamonds indicate measured loss at transparency energy.

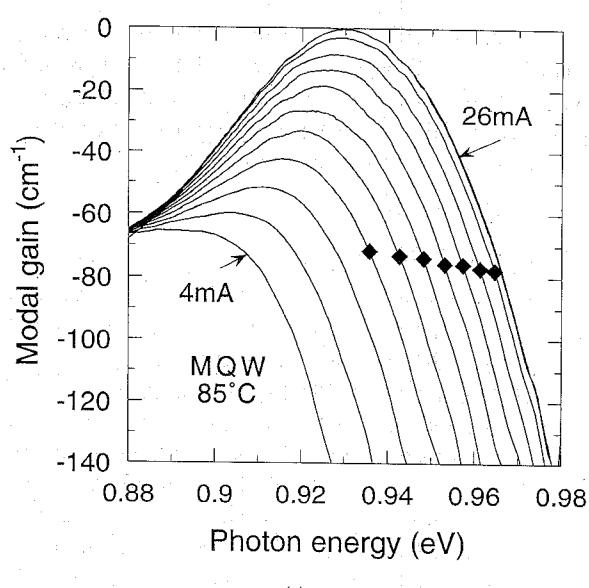

(a)

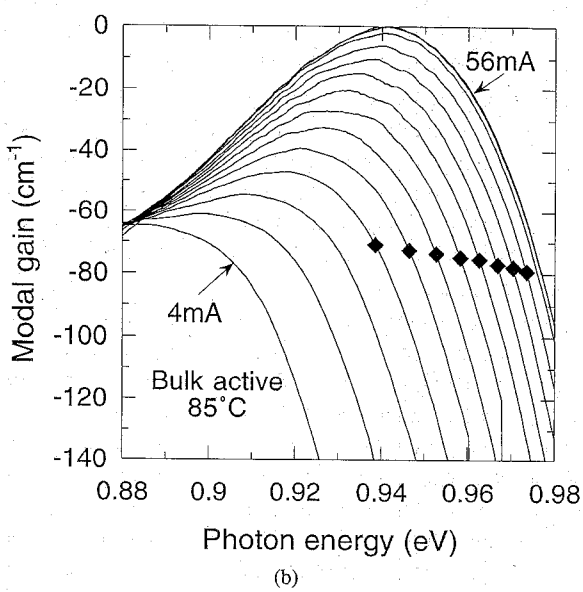

(b)

Fig. 2. Subthreshold, 85 °C modal gain spectra as a function of photon energy for (a) MQW laser for various currents (in 2 mA current steps) and (b) bulk active laser (4 mA current steps). Diamonds indicate measured loss at transparency energy.

of Fig. 5 suggest that the total recombination rate in our lasers is nearly temperature independent between 25 and 85 °C. As suggested in [19], [20], partial cancellation of temperature-related changes in radiative [32] and Auger [15], [33], [34] recombination rates over the temperature range might account for the overall temperature insensitivity observed.

Traditionally, curves such as those shown in Fig. 5 are interpreted using a polynomial fit [35] and assigning monomolecular, bimolecular and Auger recombination rates to linear (a), quadratic (b) and cubic (c) coefficients, respectively. We find that such a fitting procedure performed on our data gives large uncertainty in fit coefficients, especially in (c), that usually associated with Auger recombination. Values of $a = 0.8 \pm 0.3 \times 10^{8}$/s, $b = 0.9 \pm 0.3 \times 10^{-10}$ cm^3/s and $c = 0.7 \pm 0.4 \times 10^{-29}$ cm^6/s for MQW and $a = 1.1 \pm 0.3 \times 10^{8}$/s, $b = 2.5 \pm 0.3 \times 10^{-10}$ cm^3/s and $c = 4.7 \pm 0.6 \times 10^{-29}$ cm^6/s for bulk active lasers are obtained under the assumption that a, b, and c do not vary appreciably between 25 and 85 °C. Values for a, b, and c such as these are consistent with those found by other investigations [10], [12], [18], [29], [31]. No clear trend with temperature is observed for a, b, and c over the temperature range. Fractional deviations from a single temperature-independent fit for each of Fig. 5(a) or (b) are measured to be less than ±4%.

Mirror loss α_m is determined using the standard formula $\alpha_m \cdot L = \ln(r_1 \cdot r_2)$ in which $L \approx 300$ μm is the measured cavity length and $r_1 = r_2$ are the equal, uncoated facet field reflectivities. We used like-designed distributed feedback lasers with well defined first order grating pitch Λ and measured Bragg wavelength λ_B to obtain modal effective index $n_{\text{eff}} = \lambda_B/(2 \cdot \Lambda) = 3.25$ and we used $r_1 = (n_{\text{eff}} - 1)/(n_{\text{eff}} + 1) = 0.529$ giving $\alpha_m = -42$ cm^{-1}. Internal loss as a function of carrier density and temperature is shown in Fig. 6(a) and

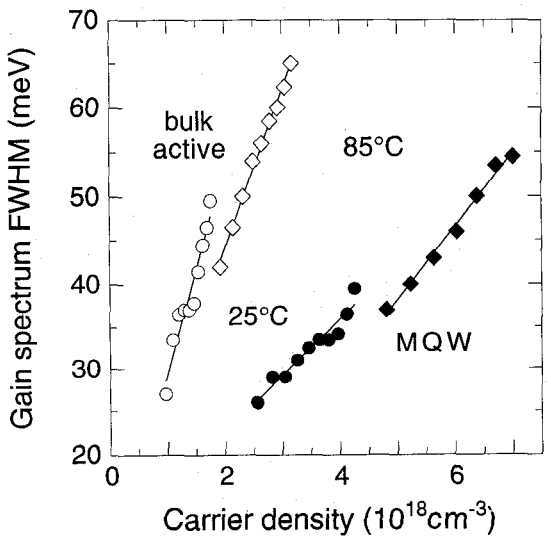

Fig. 3. Full width of gain spectrum determined at half peak net gain as function of carrier density for (a) MQW (closed symbols) and (b) bulk active laser (open symbols) at 25 °C (circles) and 85 °C (diamonds). Linear fit lines are shown.

(b) for MQW and bulk active lasers, respectively. Mirror loss was subtracted from total loss at (material) transparency, in each case. Internal loss for both MQW and bulk active lasers can be approximated for temperatures between 25 and 85 °C by a linear dependence on carrier density, independent of temperature [19], [20]. On detailed inspection, we observed a slight temperature dependence in loss at fixed carrier density. Variation in loss between 25 and 85 °C is less than 1%/K, similar in magnitude to other quaternary compounds [28]. Using calculated confinement factors of approximately 0.09 and 0.3, values of $d\alpha_{\text{int}}/dn$ of $\sim 24 \pm 5$ and $21 \pm 3 \times 10^{-18}$ cm^2 are found for MQW and bulk active material, respectively. These values are higher than the value of 13×10^{-18} cm^2 found in [28].

Net modal gain and total loss are plotted together as a function of carrier density in Fig. 7(a) and (b) for MQW and bulk active lasers, respectively. A detailed discussion of such an analysis appears elsewhere [19], [20]. We note that static differential gain, measured in the present work, was observed to agree quantitatively with that measured using relative intensity noise. Temperature dependence of differential gain dg/dn, here determined by the slope of each gain versus carrier density curve, can be fit[1] as $dg/dn(T) \propto \exp(-T/T_{0,\,dg/dn})$. $T_{0,\,dg/dn}$ falls in the range 90 to 110 K for MQW lasers and is slightly higher, 100 to 120 K, for bulk active lasers. Intersections of loss and gain curves occur at threshold carrier densities n_{th} for each temperature.

Using these intersections, threshold carrier density n_{th} can be written [19], [20][2]

$$n_{\text{th}} = \frac{\alpha_0 + n_0 \cdot dg/dn}{(dg/dn - d\alpha/dn)} \tag{1}$$

[1]See [4, Fig. 7] from which can be obtained $T_{0,\,dg/dn} \sim 135$ K, $T_{0,\,dg/dn - d\alpha/dn} \sim 85$ K.

[2]Cf. [4, (9b)].

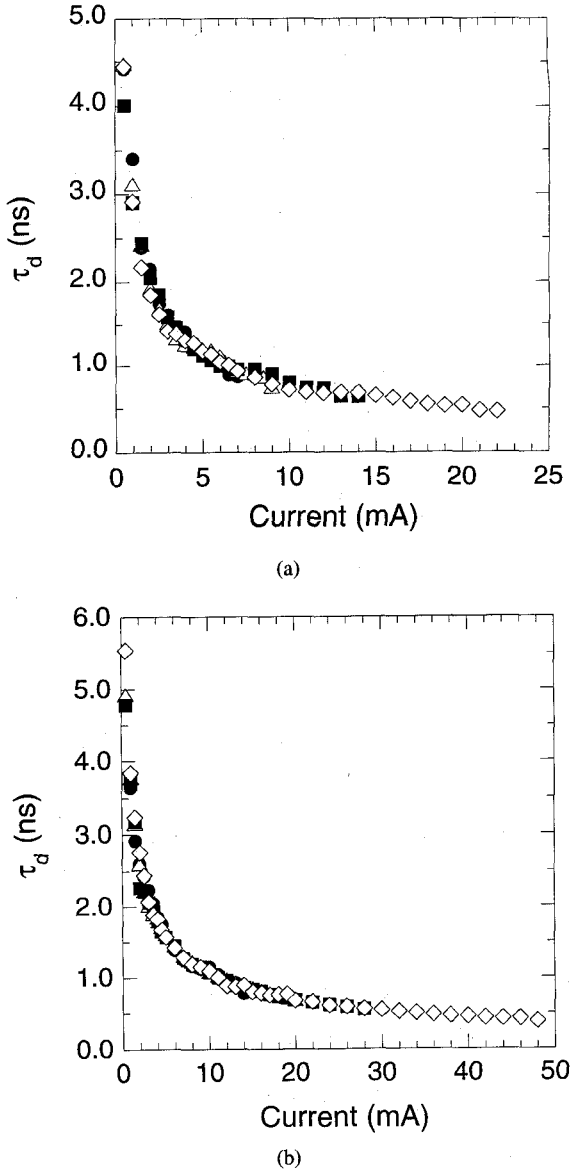

Fig. 4. Differential carrier lifetime measured as a function of current for (a) MQW and (b) bulk active laser at 25 °C (closed circles), 45 °C (open triangles), 65 °C (closed squares) and 85 °C (open diamonds).

in which α_0 is zero carrier density extrapolation of loss $\alpha(n)$, n_0 is transparency carrier density and dg/dn and $d\alpha/dn$ are differential gain and loss, respectively. Transparency carrier density n_0, which is determined by the intersection of each gain curve in Fig. 7 with zero net gain, increases with temperature [19], [20]. The product $n_0 \cdot dg/dn$ is observed to be only weakly dependent on temperature and thus, the numerator of the right-hand side of (1) is almost temperature independent. Since $dg/dn \gg d\alpha/dn$, the temperature dependence of n_{th} is approximately that of $(dg/dn)^{-1}$. By fitting measured $n_{\text{th}}(T) \propto \exp(T/T_{0,\,n_{\text{th}}})$, we determine $T_{0,\,n_{\text{th}}}$ to be approximately 120 K for MQW lasers. A slightly lower $T_{0,\,n_{\text{th}}}$ of approximately 100 K for bulk active lasers examined reflects the combination of slightly stronger temperature dependence of transparency carrier density depicted in Fig. 7(b).

At each current and temperature a transparency energy was obtained for each laser examined. Based on detailed balance

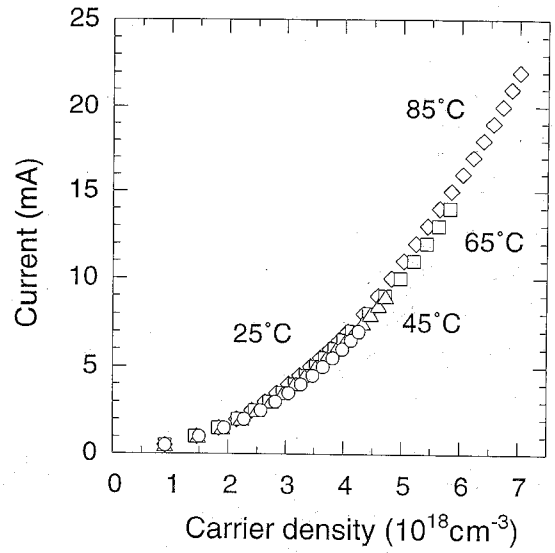

(a)

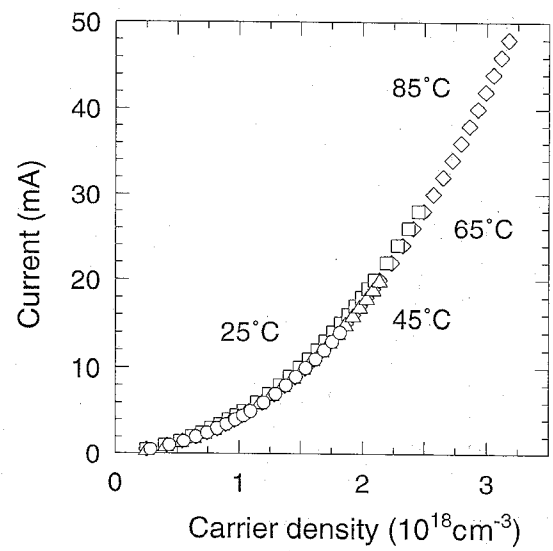

(b)

Fig. 5. Measured subthreshold current as a function of carrier density for (a) MQW and (b) bulk active laser at 25 °C (circles), 45 °C (triangles), 65 °C (squares) and 85 °C (diamonds).

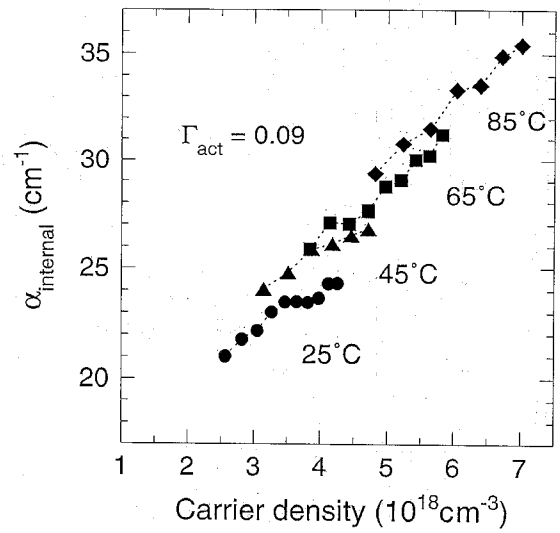

(a)

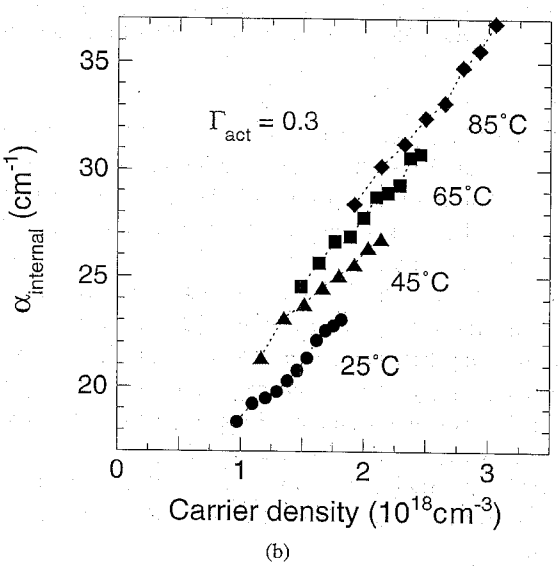

(b)

Fig. 6. Internal loss α_{internal} as a function of carrier density for (a) MQW and (b) bulk active laser at 25 °C (circles), 45 °C (triangles), 65 °C (squares) and 85 ° (diamonds). α_{int} = total measured loss $-\alpha_{\text{m}}$; α_{m} =42 cm^{-1}.

arguments, the chemical potential μ, the energy required to add an electron-hold pair to the plasma in the active region, is equal to the quasi-Fermi level separation [36], [37] and hence, to the transparency energy [38]. Fig. 8(a) and (b) show net modal gain plotted as a function of chemical potential and temperature for MQW and bulk active lasers. Lines labelled threshold in Fig. 8 represent loci of threshold net gain versus threshold chemical potential at each temperature.

For a given value of net modal gain $g(n, T)$, chemical potential $\mu(n, T)$ decreases with increasing temperature due to several factors which act simultaneously. We can approximate the change in chemical potential associated with a change in temperature and in density as $\delta\mu = \mu_{n,T} \cdot \delta n + \mu_{T,n} \cdot \delta T$, in which $\mu_{x,y}$ symbolizes the partial derivative of μ with respect to x at constant y. For a constant gain contour in Fig. 8, $-g_{n,T} \cdot \delta n = g_{T,n} \cdot \delta T$. Therefore, at a fixed gain, $\delta\mu/\delta T = -\mu_{n,T} \cdot (g_{T,n}/g_{n,T}) + \mu_{T,n} = -g_{T,n}/g_{\mu,T} + \mu_{T,n}$. Since the chemical potential can be written as the sum of the bandgap energy and the electron and hole quasi-Fermi energies (relative to each band-edge), $\mu_{T,n}$ can be conveniently decomposed into two parts. First, an increase in temperature causes a decrease in bandgap directly and hence in μ, as parameterized by standard coefficients [39]. Second, an increase of temperature affects the position of each quasi-Fermi level as carriers redistribute themselves in energy, causing a further decrease in μ dependent on the band structure. Finally, the magnitudes of $g_{T,n}$ and $g_{\mu,T}$ can be estimated from Figs. 7 and 8, respectively. The ratio $(-g_{T,n}/g_{\mu,T})$ is positive. It reflects the need for increased carrier density in order to maintain constant gain and causes μ to increase. This last effect acts with an opposite sign to that of bandgap shrinkage. Close to threshold gains, change in chemical potential with temperature $\mu_{T,g}$ is observed to be about -0.17 and -0.23 meV/K in MQW and bulk active lasers, respectively. These values are

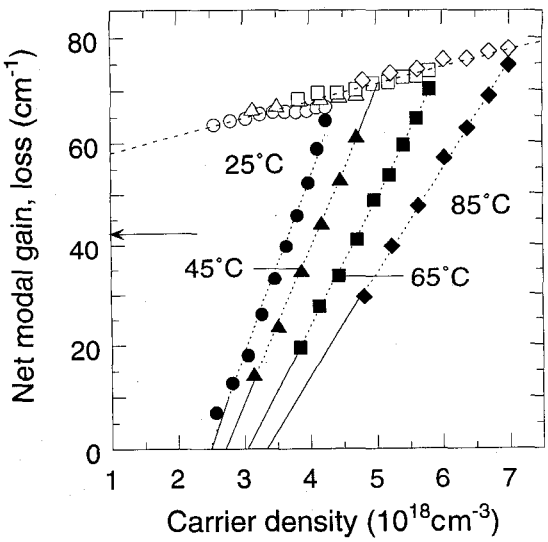

(a)

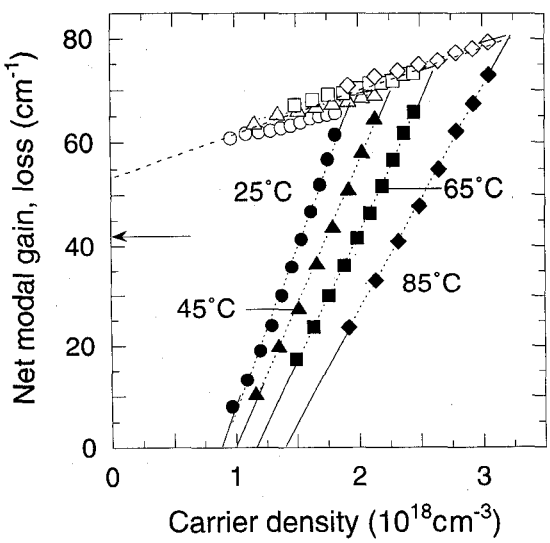

(b)

Fig. 7. Total loss (open symbols) and net modal gain (closed symbols) as a function of carrier density for (a) MQW and (b) bulk active laser at 25 °C (circles), 45 °C (triangles), 65 °C (squares) and 85 °C (diamonds). Dashed line represents single linear fit to loss data for all temperatures. Arrow indicates $\alpha_{\text{mirror}} = 42$ cm^{-1}.

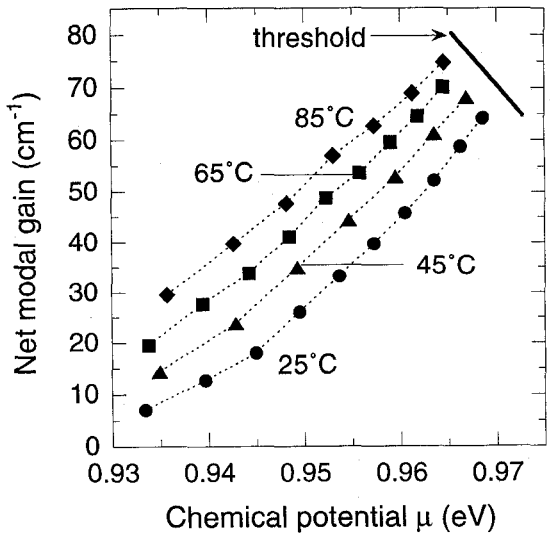

(a)

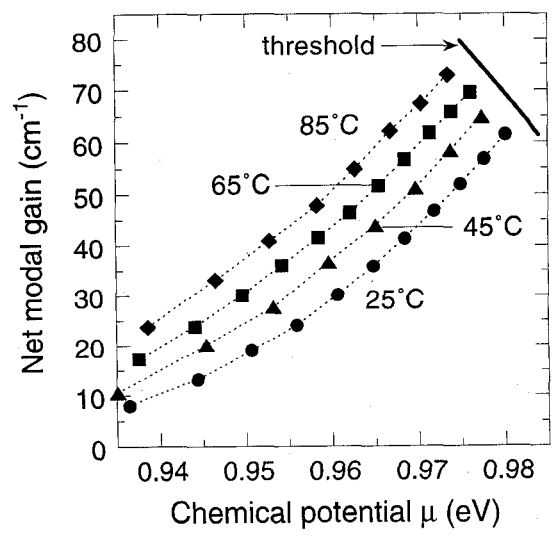

(b)

Fig. 8. Net modal gain as a function of measured chemical potential for (a) MQW and (b) bulk active laser at 25 °C (circles), 45 °C (triangles), 65 °C (squares) and 85 °C (diamonds). Solid lines represent contours of threshold gain versus threshold chemical potential. Dashed curves added as visual aid.

smaller than those predicted solely on the basis of the change of bandgap by approximately 30 to 50%. The smaller value of $\mu_{T,g}$ observed in MQW compared to bulk active lasers is probably due to a smaller value of $\mu_{T,n}$, in turn, related to the lower MQW density of states in the valence band.

We observe that slopes of net modal gain versus chemical potential increase with μ, the rate of increase slowing upon approach to threshold. The threshold value of $dg/d\mu$ decreases with increasing temperature, the overall decrease between 25 and 85 °C being greater in MQW than in bulk lasers. We note that the change of gain with chemical potential (or transparency energy) can easily be visualized using Figs. 1 or 2 by following from spectrum to spectrum, the increase of peak gain and motion of the transparency point as they each vary with current or carrier density.

Fig. 9(a) and (b) show chemical potential as a function of carrier density and temperature for MQW and bulk active lasers, respectively. As in Fig. 8, threshold contours are indicated, here showing loci of μ_{th} versus n_{th}. In Fig. 9, dashed curves represent fits of the form $\mu(n) = \mu(n_{\text{th}}) + 2k_BT \cdot \ln(n/n_{\text{th}}) + A(T) \cdot n$. This form represents the leading terms of a series approximation for the separation in quasi-Fermi levels [40] that, in the absence of the linear correction, describes the case of nondegenerate carriers with equal electron and hole densities. We observe a rapid decrease with temperature in the linear coefficient $A(T)$, which is greater than that predicted by the simple expression given in [40].

Next, we use data of Figs. 8 and 9 to probe the strong temperature dependence of differential gain at threshold. We consider modal gain $g = g(\mu(n))$ and, using the chain rule, write differential gain $g_{n,T} = g_{\mu,T} \cdot \mu_{n,T}$. Each factor is evaluated at threshold. First, we consider $g_{\mu,T}$, the rate of

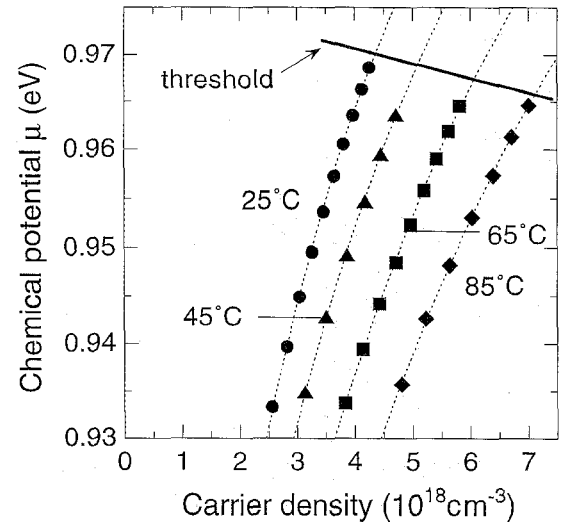

(a)

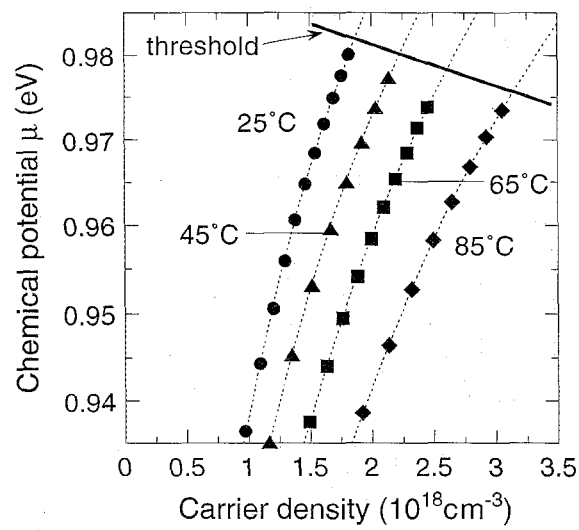

(b)

Fig. 9. Chemical potential as a function of carrier density for (a) MQW and (b) bulk active laser at 25 °C (circles), 45 °C (triangles), 65 °C (squares) and 85 °C (diamonds). Solid lines represent contours of threshold chemical potential versus threshold carrier density. Dashed curves are best fits to the form $\mu = \mu(n_{\rm th}) + 2k_BT \cdot \log(n/n_{\rm th}) + A \cdot n$, in which $A = A(T)$.

change of modal gain with chemical potential at constant temperature. This is plotted as a function of carrier density and temperature as solid symbols in Fig. 10 (in this case, for a bulk active laser). As mentioned previously, $g_{\mu,T}$ at threshold decreases with increasing temperature. At fixed gain near threshold, or at threshold gain, we observe the change of $g_{\mu,T}$ with temperature to be small, especially in bulk active lasers. For example, a drop of ~10 to 20% in threshold $g_{\mu,T}$ is seen in bulk active lasers compared to 15 to 25% in MQW lasers. Fig. 10 also shows as open symbols $\mu_{n,T}$ as a function of n and temperature. We observe that $\mu_{n,T}$ is not strongly temperature sensitive but varies rapidly with carrier density, roughly as n^{-1} as would be anticipated based on the quality of logarithmic fits of Fig. 9. For example, between 25 and 85 °C, $\mu_{n,T}$ evaluated at $n_{\rm th}(T)$ drops by approximately 50% in both MQW and bulk active lasers whereas the change in

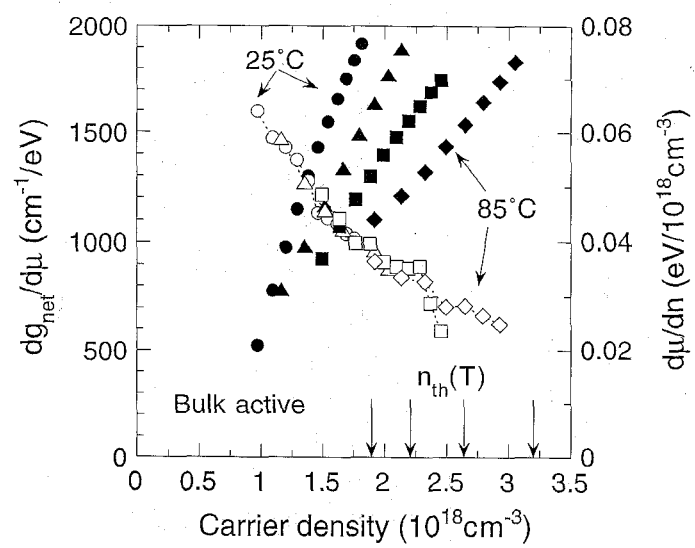

Fig. 10. Derivatives $dg/d\mu$ (closed symbols) and $d\mu/dn$ (open symbols) both as a function of carrier density for bulk active laser at 25 °C (circles), 45 °C (triangles), 65 °C (squares) and 85 °C (diamonds). Arrows indicate threshold carrier densities for each temperature. The product $(dg/d\mu \cdot d\mu/dn)$ at a given threshold carrier density yields threshold value of dg/dn.

$\mu_{n,T}$ at a fixed n, say 2×10^{18}, is small. Differentiating the expression used for fitting the data in Fig. 9 yields $\mu_{n,T} = 2k_BT/n + A(T)$. The increase with temperature of the first term is found to be largely cancelled by the decrease in the second term.

Taken together, the threshold value of $g_{\mu,T} \cdot \mu_{n,T}$ gives a differential gain at constant temperature. While $g_{\mu,T}$ evaluated at threshold does not show a very strong temperature dependence, temperature insensitive $\mu_{n,T}$ *evaluated at threshold carrier density* $n_{\rm th}(T)$ does. It is the decrease in $\mu_{n,T}$ with carrier density which amplifies the slow drop in $g_{\mu,T}$ yielding the strong, observed temperature dependence of differential gain.

III. Gain Model Results and Comparison to the Experimental Data

In order to understand the material gain in more detail, particularly the temperature sensitivity, we calculated gain for bulk quaternary InGaAsP alloys as well as MQW structures which are modeled using an extended superlattice. The approach used is summarized in the Appendix. The salient points are first, that the electronic energy levels are calculated using an envelope function approach implemented in an eight band $k \cdot p$ model. Second, the quasi-Fermi levels for electrons and holes and the allowed optical transitions are determined, from which the associated gain (absorption) is calculated. A standard independent particle model is used for the gain; many-body interaction effects due to the carrier–carrier interactions are not included explicitly. The potential impact of these interaction effects is discussed below.

The bulk active laser material is chosen to be $(In_{0.53}Ga_{0.47}As)_{0.58}(InP)_{0.42}$, approximately lattice matched to InP. This yields peak gain near 1.3 μm for material gain in the correct range. The calculation of band energies in the

alloy are standard. The eight band $k \cdot p$ model includes band nonparabolicity explicitly.

The superlattice that represents the MQW active region alternates between quaternary alloy barriers chosen to have a room temperature band gap corresponding to 1.12 μm and quaternary alloy wells of a specified strain. The well composition is tuned to achieve a room temperature superlattice band gap corresponding to the measured low energy inflection point in the photo-luminescence spectrum. Figure 11 shows the band energies and densities of states corresponding to 100-Å barriers and 70-Å wells that have 0.55% lattice mismatch with respect to InP (compressive strain in the wells). Only one electron subband is confined in the relatively shallow conduction band wells. There is a non-zero dispersion of this band along the superlattice axis, giving a quasi-three-dimensional density of states near the bottom of the subband. The higher subbands are above the barrier. They exhibit a three-dimensional contribution to the density of states that starts about 8 meV above the barrier energy. The details of the hole sub-bands depend sensitively on the choice of strain [41]–[44]. In the present case, the first two heavy hole derived subbands are separated by about 40 meV. The third subband derives from the light holes. The interaction between the first two subbands leads to noticeable nonparabolicity in the first subband and the characteristic negative curvature near $k = 0$ for the second subband. This latter feature yields a sharp spike in the density of states.

The density of states for the superlattice is compared to that of the bulk alloy in Fig. 12. The density of states is explicitly normalized by the full unit cell volume, i.e., including the barrier region in the superlattice. This contrasts with the common practice of normalizing to the well region only. However, the present approach has the advantage of comparing various designs of active region on an equivalent basis. The electron density of states in the superlattice has the same overall magnitude as that in the bulk alloy. Above the barrier, it approaches the bulk result. The electron states below the barrier will only accommodate about 8×10^{17} cm^{-3} carriers. Therefore, at room temperature and above, with typical carrier densities for laser operation, there is a significant population of electrons above the barriers in three dimensional states. In contrast, the relevant hole density of states is all confined to the well region with an effective mass and corresponding density of states substantially smaller (about a factor of three) than in the bulk case.

The temperature sensitivity of the gain has been calculated for various active layer designs. Following the experimental analysis, this degree of sensitivity is characterized by assigning a "$T_{0,n(g)}$" value. $T_{0,n(g)}$ is evaluated as follows. The peak gain is calculated as a function of electron and hole density, assumed equal, for two temperature T_1 = 25 °C and T_2 = 85 °C. Then for a given level of gain, the density required to achieve this gain is calculated at these temperatures. The temperature sensitivity is given by $T_{0,n(g)} = (T_2 - T_1)/\log(n_2/n_1)$. This is done for several different cases: bulk active and three barrier/well combinations (100 Å/70 Å with 0.55% mismatch, 100 Å/50 Å with 0.61% mismatch and 100 Å/30 Å with 0.67% mismatch). This set

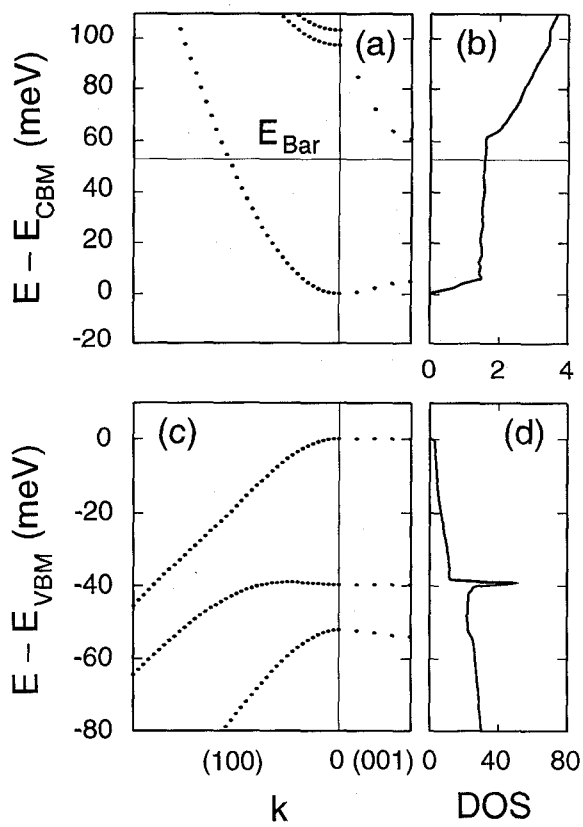

Fig. 11. Calculated band structure, (a) and (c), and density of states, (b) and (d), for a superlattice consisting of 100-Å 1.12-μm quaternary barriers and 70-Å compressively strained (0.55% lattice mismatch) quaternary wells yielding a superlattice band gap of 1.3 μm. Energies are taken relative to the respective band edges. The position of the barrier conduction band is indicated. The range of in-plane k-vector is 5% of the Brillouin zone while the k-vector along the axis extends to the superlattice zone boundary. The units for the density of states are 1×10^{19} states/eV/cm^3.

of cases is by no means exhaustive, but covers the range of devices included in the present experimental study. For each case, the value of material gain required is varied from 50 cm^{-1} to $g_{\max}$, a few times usual threshold value. (The $g_{\max}$ was 1000, 2700, 3000, and 2300 cm^{-1} for the bulk, 30, 50, and 70 Å cases, respectively, normalized to be gain per well.) For the superlattice structures, the value of gain and carrier density are also taken relative to the full unit cell volume, i.e., including the barrier regions. This view allows easy comparison among various designs imagining that the total active layer thickness is invariant. Results are plotted in Fig. 13 showing calculated $T_{0,n(g)}$ versus density to achieve g at 25 °C. The first obvious point is that this model does not give agreement with the magnitude of T_0 found experimentally and analyzed in the previous section. This general situation is well known [18]–[20]. However, it is interesting that the model does predict definite changes in temperature sensitivity with structure and demanded gain, or operating point. In fact, the range of variation found in Fig. 13 of about 25% is similar to that observed between the bulk active and MQW measured $T_{0,dg/dn}$ with the latter being more temperature sensitive.

The bulk material shows a steady rise in T_0 with carrier density. The superlattices exhibit a weak maximum. In order to understand this better, the case of ideal quantum wells is

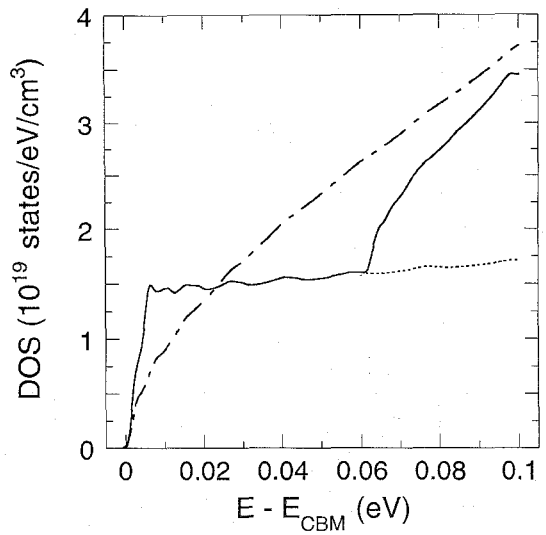

(a)

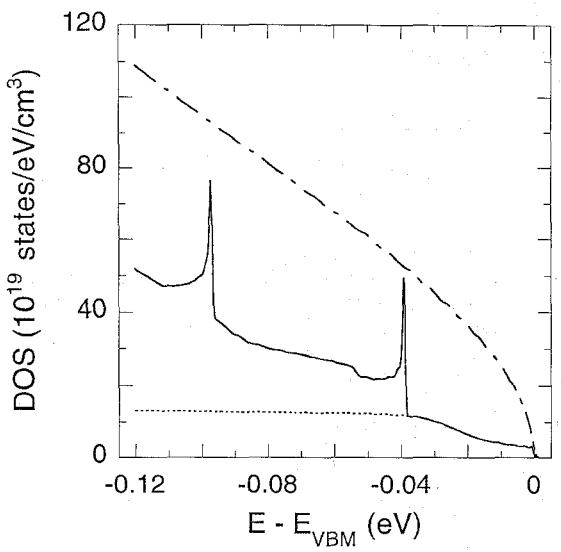

(b)

Fig. 12. Comparison of the density of states calculated for the superlattice in Fig. 11 (solid) to that of the bulk quaternary alloy with 1.3-μm band gap (dash-dot) for (a) the electron states and (b) hole states near the region of the fundamental gap. Dashed lines indicate the contribution of the first subband.

considered. With only a single electron and hole subband, the peak gain as a function of temperature and density can be calculated analytically [14]. The relation $n_1/T_1 = n_2/T_2$ must be satisfied in order to maintain constant gain as a function of temperature. Thus, $T_0 = T$, or for the finite difference case, approximately the average of T_1 and T_2. A line at $T_0 = 330$ K independent of the demanded gain, or operating carrier density is shown in Fig. 13. The two aspects of the density of states that yield this result are the abrupt step at the band edge and the constant value beyond. In particular, while maintaining constant gain with increasing temperature, there is no change of the quasi-Fermi levels for electrons and holes.

Next, we consider a realistic density of states for the electrons and holes, but exclude the higher subbands. Resultant values of $T_{0,n(g)}$ are plotted as the curve labeled "2 bands only" in Fig. 13. This more realistic density of states adds

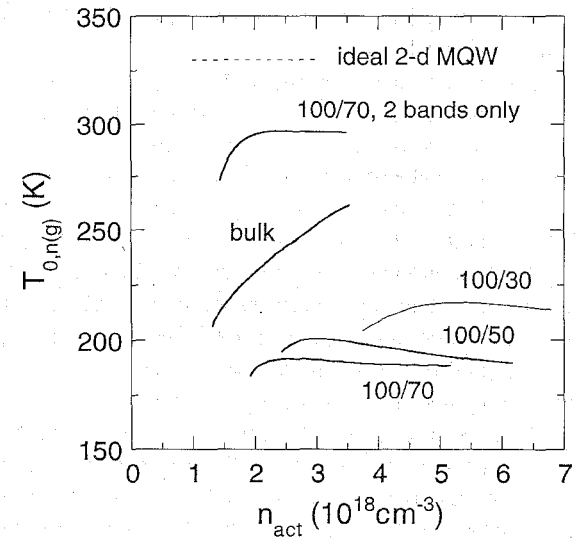

Fig. 13. Calculated $T_{0,n(g)}$ as a function of room temperature carrier density required to maintain a constant material gain value g. 100/70 notation refers to barrier/well thickness in Å.

two additional features. First, the nonparbolicity leads to a nonconstant density of states. The additional state density in the tail of the carrier distribution demands additional carriers to maintain given quasi-Fermi levels, and hence gain. The demand for additional carriers translates to increases temperature sensitivity. T_0 is reduced to the range of 280 K. Furthermore, as the operating carrier density or demanded gain increases, the need for more carriers increases, producing a slight negative slope in $T_{0,n(g)}$ for higher densities. Second, the density of states for the electrons no longer has an abrupt step at the band edge. Therefore the gain spectrum no longer rises abruptly at the band gap, but has a smooth rise as found for a bulk material. The initial tendency for T_0 to rise with density in the superlattice materials follows the same trend for the bulk material seen in Fig. 13. This observation is supported by the fact that the rise is more pronounced for the material with 30-Å wells where the superlattice dispersion of the electron sub-band is larger.

Finally, when the additional subbands are included in the calculation, T_0 drops into the range of 180–220 K. The extra states are populated in the thermal distribution of carriers, but do not contribute to the gain. This is a substantial efffect for the electrons, and non-negligible for the holes as well. The second hole subband in Fig. 12 has a large state density associated with it. Furthermore, there is a systematic trend showing the energy of this sub-band dropping (becoming more negative) as the well width is reduced. Consideration of this trend has previously been identified as important in design of MQW active layer material [41]–[43]. In the present structures, the hole subband moves from -40 meV (70 Å wells) to -80 meV (30 Å wells). At the same time, the capacity of the bound electron subband increases by about 20%. Together, these changes in the subband structure increase the range of T_0 from 180 K to 220 K. These results show that there is some room for altering the temperature sensitivity of the gain through changes in MQW design. However, the overall influence of the higher subbands remains quite important.

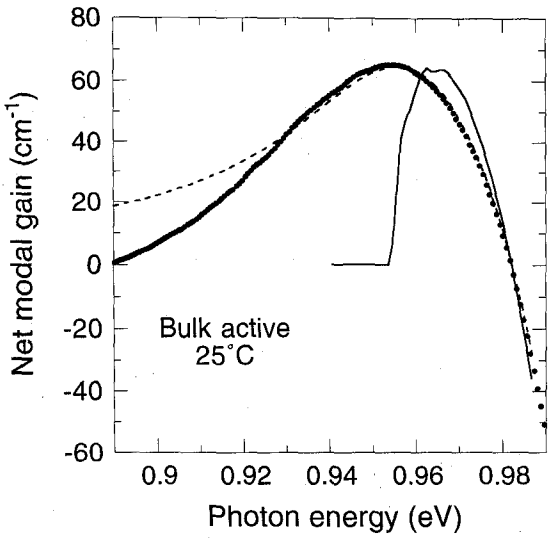

Fig. 14. Gain spectrum near threshold at 25 °C for the bulk active device. Experiment (dots), calculation without broadening (solid line) and calculation with Lorentzian broadening (dashed line) are described in the text.

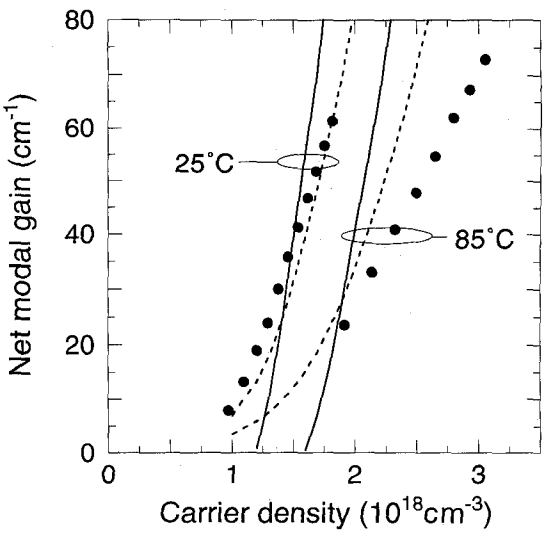

Fig. 15. Comparison of calculated peak modal gain versus carrier density to experiment for the bulk active device at the indicated temperatures. Experiment (dots), calculation without broadening (solid line) and calculation with Lorentzian broadening (dashed line) are described in the text.

The model calculations do not yield the same degree of temperature sensitivity of gain as found in the devices. We now turn to a more detailed comparison with the data. In Fig. 14, the modal gain spectrum is shown for a bulk active device biased just below the threshold. Using a calculated modal confinement factor of $\Gamma_{\rm act} \cong 0.3$, the corresponding calculated gain spectrum is shown. The spectra have been aligned at transparency, involving a shift of the calculated spectrum by about 20 meV toward lower energy. The model is clearly inadequate in two respects: first, the peak of the gain is too close to the transparency energy and secondly, the width on the low energy side is substantially too small. One consequence of the carrier–carrier interactions is a finite lifetime, or homogeneous broadening, in the gain curve. This dephasing time is typically taken to be 0.1 ps [42], [43], while more detailed calculations suggest 0.05–0.1 ps [45]. However, the resultant Lorentzian broadening (about 5–10 meV half width) is insufficient to explain the observed width of the gain peak as measured. For consistency, broadening has been applied to the spontaneous emission spectrum from which the gain is then derived [36], [37]. A half width of 25 meV is required to approximate the peak position and width, as shown by the dashed curve in Fig. 14. However, this large amount of broadening introduces an unphysical low energy tail. If a similar fit is made to the spectrum at 85 °C, an even larger broadening parameter of 33 meV is required. Finally, this larger Lorentzian broadening can give the correct separation between the chemical potential and the peak of the gain curve, across the range of carrier density. However, the data of Fig. 3 (measured FWHM of the gain curves) support the need for density dependent broadening.

The calculated variation of peak modal gain with carrier density is compared to the experimental results in Fig. 15. Two points of disagreement are evident: first, the calculated slopes are too large and secondly, the change of threshold density and differential gain with temperature is substantially underestimated. These discrepancies cannot be removed through homogeneous broadening, even allowing for a temperature dependant broadening as derived from the fits described above. The slope at 25 °C is improved, providing reasonable agreement, but changes with temperature are still too small.

Following the break up of the differential gain into a dependence of $g(\mu)$ and $\mu(n)$, the model calculations are compared to the experiments in Figs. 16 and 17. The temperature dependence of the band gap has been explicitly included in the model for the chemical potential difference. As in Fig. 15, the band gap has also been shifted to align the chemical potential to the experimental transparency energy at the 25 °C threshold. In the absence of broadening, the gain rises too quicky with increasing chemical potential difference. With reference to the inset in Fig. 16 and the discussion of Fig. 8, the change of μ with temperature has two parts. First, the bandgap, and hence the separation of quasi-Fermi levels decreases with increasing temperature. Second, to achieve a given value of gain, the quasi-Fermi levels must move into (towards) the bands, thus increasing μ. This latter effect is the net result of changes in μ with temperature and an increase in density and is underestimated by the model. On the other hand, the temperature sensitivity of the slope $dg/d\mu$ is quite weak, and similar to that which is measured. Introduction of homogeneous broadening, with values of broadening fit to our experiments near threshold (at each temperature, but constant with density), yields a reasonable agreement with experimental values of $g(\mu)$ in the range shown. This agreement can be largely attributed to the gain transferred to energies below the band gap by the broadening. Unfortunately, the long low energy tail noted in Fig. 14 is here converted into gain extending far below the band gap that is not observed experimentally.

The most surprising result is that the temperature sensitivity of the chemical potential is not reproduced in the band model. The density dependence at 25 °C is approximately

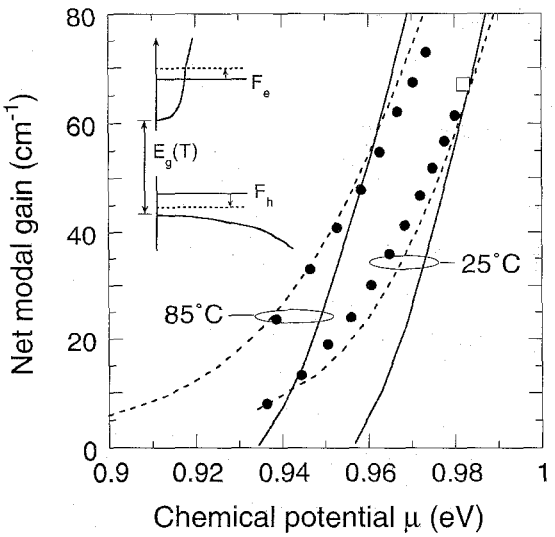

Fig. 16. Same as Fig. 15 for the peak modal gain versus chemical potential. The calculated chemical potential is aligned to experiment at 25 °C shown by the open square. The inset illustrates the changes in the chemical potential with temperature required to maintain constant gain.

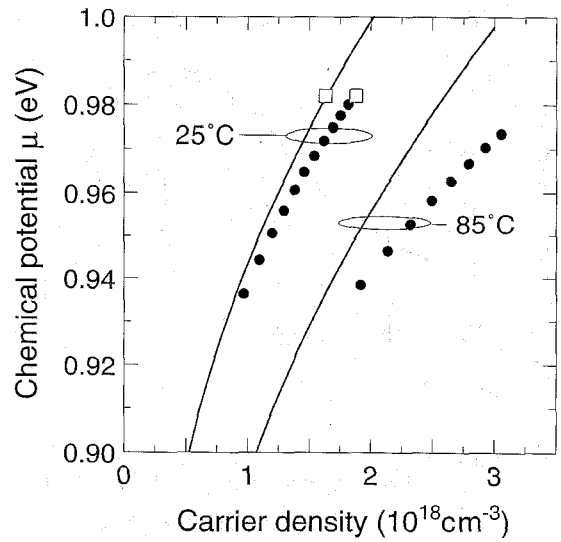

Fig. 17. Comparison of calculated chemical potential versus carrier density to experiment for the bulk active device at the indicated temperatures. Experiment (dots) and calculation (solid line) are described in the text. The open squares show the chemical potential at 25 °C threshold.

correct. However, the change when temperature is increased to 85 °C is not well represented. Several empirical schemes have been examined to understand this situation. Usually, one expects band tails in the gap region due to disorder, e.g., from alloy fluctuations. However, inclusion of gaussian broadening of the density of states (up to 50 meV) prior to calculation of the quasi-Fermi levels for electrons and holes does not substantially alter Fig. 17. A second possible omission from the model is background doping in the active region. This is most likely p-type with an upper bound of about 5×10^{17} cm^{-3}. Inclusion of extra holes shifts the curves for $\mu(n)$ upward providing neither closer to agreement nor improved temperature sensitivity.

A third omission from the model, as presented in Figs. 15–17, is many-body corrections. Model calculations exist for the many-body correction to the chemical potential showing red shifts of 20 to 30 meV with a weak density dependence [46]–[48]. Incorporation of this correction, which would give a small change in Fig. 17, tends to improve the dependence on density in comparison to the experimental data. There should also be an overall enhancement of the modal gain. For the present densities, this factor should be less than about 1.3, and again weakly dependent on density [46]–[48]. We do not expect this to be sufficient to change the temperature sensitivity of the model. The homogeneous broadening should be both density and temperature dependent. This will also slightly alter the curves in Figs. 15 and 16. But as seen in the discussion above, the broadening needed to explain the measured width of the gain spectra is too large to be plausibly explained by a homogeneous broadening.

The possible presence of background doping raises the related issue of inhomogeneous broadening. The impurity centers represent extra scattering which produces band tails and alters the low energy gain through the breakdown of the k-selection rule for the optical transitions. A detailed model has been described for this case of high doping density [49]–[50]. Qualitatively, this will lead to enhanced gain at lower carrier density, while approaching the present results at higher density where k-selection is approximately obeyed. In the present materials system, there is the additional influence of alloy disorder, as well as the possibility for longer wavelength compositional fluctuations such as spinodal decomposition [51]. For the MQW structures, well width variation represents another source of inhomogeneous broadening. Quantitative modeling of these effects appears to be quite relevant for understanding the experimental data.

IV. Conclusion

Extensive experimental characterization of 1.3-μm MQW and bulk active lasers has been performed to investigate the temperature sensitivity of threshold. We have presented evidence indicating that the temperature sensitivity of gain dominates other mechanisms, among them non-radiative recombination and optical loss, thereby playing a pivotal role in reducing T_0 of both 1.3-μm MQW and bulk active lasers. Using measured chemical potential μ, we can examine the temperature dependence of differential gain dg/dn as that of the product $dg/d\mu \cdot d\mu/dn$. Of these two measured factors, the first $dg/d\mu$ is characterized by a slow drop with temperature at threshold. The latter quantity $d\mu/dn$ is observed to be only weakly temperature dependent but strongly carrier density dependent. Together, these factors produce a strongly temperature dependent differential gain which we characterize with $|T_{0,\,dg/dn}| = 90$ to 120 K. Threshold carrier density is shown to possess in magnitude a very similar and strong temperature dependence. We note that the nonlinear current–carrier density relationship, which is measured, provides a conversion of $T_{0,\,dg/dn}$ to the more familiar parameter $T_0 \cong 55$ K.

Temperature sensitivity of gain has been analyzed using a model which includes detailed band structure calculations for each MQW and bulk active case. The model does not predict the observed value of T_0. However, the model does explain the variation of temperature sensitivity with structure between MQW and bulk active lasers. Comparison of the calculated to the measured gain spectra highlights the importance of broadening. We expect that a degree of homogeneous broadening as well as inhomogeneous broadening due to material fluctuations is required in order for the model to provide a more realistic picture of T_0 in long wavelength semiconductor lasers.

APPENDIX
DESCRIPTION OF THE GAIN MODEL

The eight band $k \cdot p$ model describes the bulk semiconductor energy bands in the region of the fundamental band gap including the heavy hole, light hole and split-off hole bands as well as the lowest conduction band near the $k = 0$ point in the Brillouin zone. The spin-orbit interaction is fully included. The influence of strain on the band structure is incorporated through the conventional deformation potentials [52]. This model is extended to the heterostructure case through the use of the standard envelope function approximation. The MQW structures are represented by an extended superlattice which allows periodicity to be exploited in calculating the band energies and wavefunctions. A detailed description of this method is provided in [41] and [53]. We used that approach as a starting point, but included some new features.

The calculation of the band energies, wavefunctions and dipole matrix elements follows [41] and [53] closely. The band structure is calculated at $T = 0$ using the low temperature band gap is input. Then the band structure is rigidly shifted according to the experimental band gap change with temperature as described by the Varshni coefficients [39]. The Luttinger parameters for InP are taken to be $\gamma_1 = 5.15$, $\gamma_2 = 0.94$, and $\gamma_3 = 1.62$ [54]. The deformation potentials are taken from [55]. Parameters needed for the $In_xGa_{1-x}As$ strained alloys are expanded linearly about those for the lattice matched alloy. The needed Luttinger parameters are interpolated or extrapolated from the well known values for GaAs [56] and the lattice matched alloy [57]. The tabulated values for InAs, which are far from the linear extrapolation, are not used. Finally, the needed band offset is calculated using the scheme in [55]. One should note that in the present formulation, only the effective dipole contribution to the offset enters the envelope function equations explicitly. Contributions due to differences in strain and spin-orbit splitting enter through other terms which explicitly appear in the eight band Hamiltonian. In the notation of [55], the ΔE_v^{avg} enters. At this time, self consistent calculations for pumped material have not been done. This might be significant if there is sufficient separation of electrons and holes in the superlattice, i.e., due to electron occupancy of states above the barrier.

The density of states near the band gap is calculated from the band energies using the linear tetrahedron method [58]. A three-dimensional sampling is retained for the superlattice case to fully account for dispersion along the superlattice axis as well as resonances above the barrier. This requires a Brillouin zone mesh covering the irreducible wedge near the $k = 0$ point. Since the energy range is quite small for the gain problem, a rather dense mesh is required. A spacing of about 0.5% of the Brillouin zone dimension (or about 0.005 Å^{-1}) has typically been used. The residual small scale fluctuations in Fig. 12 reflect the degree of sampling error. Similarly, the linear gain is also calculated with this method. Again, due to the small energy range as well as the rather small scale of gain in comparison to absorption in unpumped material, care must be taken to have a sufficiently fine mesh. In addition, it is essential to linearly interpolate the dipole matrix elements inside the tetrahedra. This closely preserves the transparency energy, which must be equal to the difference in electron and hole quasi-Fermi levels. The unbroadened gain spectrum in Fig. 14 exhibits some fine scale structure near the peak which is attributable to errors introduced by the Brillouin zone mesh size.

Homogeneous broadening due to electron-hole dephasing can be introduced through a Lorentzian line shape. However, the result is a general one in that the transparency energy equal the difference in quasi-Fermi levels [36], [37]. This is preserved by applying the broadening to the spontaneous emission spectrum. Then gain is derived through the relation

$$R_{sp}(E) = -\frac{\left(\frac{8\pi}{h}\right)\left(\frac{n_g E}{hc}\right)^2 \cdot g(E)}{e^{(E-\mu)/(kT)} - 1}.$$

ACKNOWLEDGMENT

The authors gratefully acknowledge the help of K. Kojima, V. Swaminathan, J. Stayt, and J. Freund for supplying some of the devices for this study.

REFERENCES

[1] J. I. Pankove, "Temperature dependence of emission efficiency and lasing threshold in laser diodes," *IEEE J. Quantum Electron.*, vol. 4, pp. 119–122, 1968.
[2] A. R. Adams, M. Asada, Y. Suematsu, and S. Arai, "The temperature dependence of the efficiency and threshold current of $In_{1-x}Ga_xAs_yP_{1-y}$ lasers related to intervalence band absorption," *Jap. J. Appl. Phys.*, vol. 19, pp. L621–L624, 1980.
[3] M. Asada, A. R. Adams, K. E. Stubkjaer, Y. Suematsu, Y. Itaya, and S. Arai, "The temperature dependence of the threshold current of GaInAsP/InP DH lasers," *IEEE J. Quantum Electron.*, vol. QE-17, pp. 611–619, 1981.
[4] M. Asada and Y. Suematsu, "The effects of loss and nonradiative recombination of the temperature dependence of threshold current in 1.5–1.6 μm GaInAsP/InP lasers," *IEEE J. Quantum Electron.*, vol. QE-19, pp. 917–923, 1983.
[5] M. Yano, H. Nishi, and M. Takusagawa, "Temperature characteristics of theshold current in InGaAsP/InP double heterostructure lasers," *J. Appl. Phys.*, vol. 51, pp. 4022–4028, 1980.
[6] Y. Horikoshi and Y. Furukawa, "Temperature sensitive threshold current of InGaAsP-InP double heterostructure lasers," *Jap. J. Appl. Phys.*, vol. 18, pp. 809–815, 1979.
[7] G. B. H. Thompson and G. D. Henshall, "Nonradiative carrier loss and temperature sensitivity of threshold in 1.27 μm (GaIn)(AsP)/InP D.H. Lasers," *Electron. Lett.*, vol. 16, pp. 42–44, 1980.
[8] A. Sugimura, "Band-to-band Auger recombination in InGaAsP lasers," *Appl. Phys. Lett.*, vol. 39, pp. 21–23, 1981.
[9] T. Uji, K. Iwamoto and R. Lang, "Nonradiative recombination in InGaAsP/InP light sources causing light emitting diode output saturation

and strong laser-threshold-current temperature sensitivity," *Appl. Phys. Lett.,* vol. 38, pp. 193–195, 1981.

[10] N. K. Dutta and R. J. Nelson, "Temperature dependence of the lasing characteristics of the 1.3 μm InGaAsP-InP and Ga-As-A10.36Ga0.64As DH lasers," *IEEE J. Quantum Electron.,* vol. 18, pp. 871–878, 1982.

[11] N. K. Dutta and R. J. Nelson, "The case for Auger recombination in $In_{1-x}Ga_xAs_yP_{1-y}$," *J. Appl. Phys.,* vol. 53, pp. 74–92, 1982.

[12] A. Mozer, K. M. Romanek, O. Hildebrand, W. Schmid, and M. H. Pilkuhn, "Losses in GaInAs(P)/InP and GaAlSb(As)/GaSb lasers—The influence of the split-off valence band," *IEEE J. Quantum Electron.,* vol. QE-19, pp. 913–916, 1983.

[13] A. P. Mozer, S. Hausser, and M. H. Pilkuhn, "Quantitative evaluation of gain and losses in quaternary lasers," *IEEE J. Quantum Electron.,* vol. QE-21, 719–725, 1985.

[14] E. P. O'Reilly and M. Silver, "Temperature sensitivity and high temperature operation of long wavelength semiconductor lasers," *Appl. Phys. Lett.,* vol. 63, pp. 3318–3320, 1993.

[15] M. C. Wang, K. Kash, C. E. Zah, R. Bhat, and S. L. Chuang, "Measurement of nonradiative and radiative recombination rates in strained-layer quantum-well systems," *Appl. Phys. Lett.,* vol. 62, pp. 166–168, 1993.

[16] P.-L. Liu, J. P. Heritage, and O. E. Martinez, "Temperature dependence of the threshold current of an InGaAsP laser under 130-ps electrical pulse pumping," *Appl. Phys. Lett.,* vol. 44, pp. 370–372, 1983.

[17] N. K. Dutta and N. A. Olsson, "Temperature dependence of threshold current of injection lasers for short pulse excitation," *Appl. Phys. Lett.,* vol. 44, pp. 943–944, 1984.

[18] Y. Zou, J. S. Osinski, P. Grodzinski, P. D. Dapkus, W. C. Rideout, W. F. Sharfin, J. Schlafer, and F. D. Crawford, "Experimental study of Auger recombination, gain, and temperature sensitivity of 1.5 μm compressively strained semiconductor lasers," *IEEE J. Quantum Electron.,* vol. 29, pp. 1565–1575, 1993.

[19] D. A. Ackerman, P. A. Morton, R. F. Kazarinov, T. Tanbun-Ek, and R. A. Logan, "Analysis of T_0 in 1.3 μm multi-quantum well and bulk active lasers," in *Proc. InP and Related Materials Conf.,* Santa Barbara, CA, 1994, pp. 466–468.

[20] D. A. Ackerman, P. A. Morton, G. E. Shtengel, M. S. Hybertsen, R. F. Kazarinov, T. Tanbun-Ek, and R. A. Logan, "Analysis of T_0 in 1.3 μm multi-quantum-well and bulk active lasers," *Appl. Phys. Lett.,* accepted for publication.

[21] R. F. Nabiev, E. C. Vail, C. J. Chang-Hasnian, and W.-P. Yuen, "Temperature behavior of 980 nm Al-free single and triple-strained quantum well lasers," in *Conf. Lasers and Electro-Opt., Tech. Dig.,* Anaheim, CA, 1994, p. 27.

[22] J. L. Zilko, L. J. P. Ketelsen, Y. Twu, D. P. Wilt, S. G. Napholtz, J. P. Blaha, K. E. Strege, V. G. Riggs, D. L. Vanharen, S. Y. Leung, P. M. Nitzsche, J. A. Long, G. Przyblek, J. Lopata, M. W. Focht, and L. A. Koszi, "Growth and characterization of high yield, reliable, high-power, high-speed InP/InGaAsP capped mesa buried heterostructure distributed feedback lasers," *IEEE J. Quantum Electron.,* vol. 25, pp. 2091–2095, 1989.

[23] R. F. Kazrinov and M. R. Pinto, "Carrier transport in laser heterostructures," *IEEE J. Quantum Electron.,* vol. 30, pp. 49–53, 1991.

[24] B. W. Haaki and T. L. Paoli, "Gain spectra in GaAs double-heterostructure injection lasers," *J. Appl. Phys.,* vol. 46, pp. 1299–1306, 1975 (and reference 1 cited therein).

[25] D. T. Cassidy, "Technique for measurement of the gain spectra of semiconductor laser diodes," *J. Appl. Phys.,* vol. 56, pp. 3096–3099, 1984.

[26] P. A. Andrekson, N. A. Olsson, T. Tanbun-Ek, R. A. Logan, D. L. Coblentz, and H. Temkin, "Novel technique for determining internal loss of individual semiconductor lasers," *Electron. Lett.,* vol. 28, pp. 171–172, 1992.

[27] G. E. Shtengel and D. A. Ackerman, "Internal optical loss measurements in 1.3 μm InGaAsP lasers," *Electron. Lett., submitted.*

[28] C. H. Henry, R. A. Logan, F. R. Merritt, and J. P. Luongo, "The effect of intervalence band absorption on the thermal behavior of InGaAsP lasers," *IEEE J. Quantum Electron.,* vol. QE-19, pp. 947–952, 1983.

[29] R. Olshansky, J. LaCourse, T. Chow, and W. Powazinik, "Measurement of radiative, Auger and nonradiative currents in 1.3 μm InGaAsP buried heterostructure lasers," *Appl. Phys. Lett.,* vol. 50, pp. 310–312, 1987.

[30] G. E. Shtengel, D. A. Ackerman, P. A. Morton, E. J. Flynn, and M. S. Hybertsen, "Independance-corrected carrier lifetime measurements in semiconductor lasers," *Appl. Phys. Lett., submitted.*

[31] G. H. B. Thompson, "Analysis of radiative and nonradiative recombination in lightly doped InGaAsP lasers," *Electron. Lett.,* vol. 19, pp. 154–155, 1983.

[32] A. Ghiti, M. Silver, and E. P. O'Reilly, "Low threshold current and high differential gain in ideal tensile- and compressive-strained quantum-well lasers," *J. Appl. Phys.,* vol. 71, pp. 4626–4628, 1992.

[33] W. W. Lui, T. Yamanaka, Y. Yoshikuni, S. Seki, and K. Yokoyama, "Unifying explanation for recent temperature sensitivity measurements of Auger recombination effects in strained InGaAs/InGaAsP quantum-well lasers," *Appl. Phys. Lett.,* vol. 63, pp. 1616–1618, 1993.

[34] G. Fuchs, C. Schiedel, A. Hangleiter, V. Harle, and F. Schotz, "Auger recombination in strained and unstrained InGaAs/InGaAsP multiple quantum-well lasers," *Appl. Phys. Lett.,* vol. 62, pp. 396–398, 1993.

[35] J. Heinen, H. Albrecht, and C. Weyrich, "Determination of the recombination coefficients in undoped (In, Ga)(As, P) from transient optical analysis of (In, Ga)(As, P)-InP double heterostructure LED's, *J. Appl. Phys.,* vol. 53, pp. 1800–1803, 1982.

[36] C. H. Henry, R. A. Logan, and F. R. Merritt, "Measurement of gain and absorption spectra in AlGaAs buried heterostructure lasers," *J. Appl. Phys.,* vol. 51, pp. 3042–3050, 1980.

[37] H. Haug and S. Schmitt-Rink, "Electron theory of the optical properties of laser-excited semiconductors," *Proc. Quantum Electron.,* vol. 9, pp. 3–100, 1984.

[38] M. G. A. Bernard and G. Duraffourg, "Laser conditions in semiconductors," *Phys. Status Solidi,* vol. 1, pp. 699–703, 1961.

[39] H. Temkin, V. G. Keramidas, M. A. Pollack, and W. R. Wagner, "Temperature dependence of photoluminescence of n-InGaAsP," *J. Appl. Phys.,* vol. 52, pp. 1574–1578, 1981.

[40] W. B. Joyce and R. W. Dixon, "Analytic approximations for the Fermi energy of an ideal Fermi gas," *Appl. Phys. Lett.,* vol. 31, 354–356, 1977.

[41] D. Gershoni, C. H. Henry, and G. A. Baraff, "Calculating the optical properties of multidimensional heterostructures: Application to the modeling of quaternary quantum well lasers," *IEEE J. Quantum Electron.,* vol. QE-29, pp. 2433–2450, 1993.

[42] S. Seki and K. Yokoyama, "Strain and quantum-confinement effects on differential gain of strained InGaAsP/InP quantum well lasers," *J. Appl. Phys.,* vol. 74, pp. 4242–4244, 1993.

[43] S. Seki, T. Yamanaka, W. Lui, Y. Yoshikuni and K. Yokoyama, "Theoretical analysis of pure effects of strain and quantum confinement on differential gain in InGaAsP/InP strained-layer quantum-well lasers," *IEEE J. Quantum Electron.,* vol. QE-30, pp. 500–510, 1994.

[44] D. Ahn and S. L. Chuang, "The theory of strained-layer quantum-well lasers with bandgap renormalization," *IEEE J. Quantum Electron.,* vol. 30, pp. 350–365, 1994.

[45] R. Binder, D. Scott, A. E. Paul, M. Lindberg, K. Henneberger, and S. W. Koch, "Carrier-carrier scattering and optical dephasing in highly excited semiconductors," *Phys. Rev. B,* vol. 45, pp. 1107–1115, 1992.

[46] P. Vashishta, S. G. Das, and K. S. Singwi, "Thermodynamics of the electron-hole liquid in Ge, Si, and GaAs," *Phys. Rev. Lett.,* vol. 33, pp. 911–914, 1974.

[47] P. Vashishta, P. Bhattacharyya, and K. S. Singwi, "Electron-hole liquid in many-band systems. I. Ge and SI under large uniaxial strain," *Phys. Rev. B,* vol. 10, pp. 5108–5126, 1974.

[48] X. Zhu, M. S. Hybertsen, and P. B. Littlewood, unpublished.

[49] F. Stern, "Effect of band tails on stimulated emission of light in semiconductors," *Phys. Rev.,* vol. 148, pp. 186–194, 1966.

[50] H. C. Casey, Jr. and F. Stern, "Concentration-dependent absorption and spontaneous emission of heavily doped GaAs," *J. Appl. Phys.,* vol. 47, pp. 631–643, 1976.

[51] S. N. G. Chu, S. Nakahara, K. E. Strege, and W. D. Johnston, Jr., "Surface layer spinodal decomposition in $In_{1-x}Ga_xAs_yP_{1-y}$ and $In_{1-x}Ga_xAs$ grown by hydride transport vapor-phase epitaxy," *J. Appl. Phys.,* vol. 57, pp. 4610–4615, 1985.

[52] T. B. Bahder, "Eight-band $k \cdot p$ model of strained zinc-blende crystals," *Phys. Rev. B,* vol. 41, pp. 11992–12001, 1990 and Erratum, *Phys. Rev. B,* vol. 46, p. 9913, 1992.

[53] G. A. Baraff and D. Gershoni, "Eigenfunction-expansion method for solving the quantum-wire problem: Formulation," *Phys. Rev. B,* vol. 43, pp. 4011–4022, 1991.

[54] P. Rochon and E. Fortin, "Photovoltaic effect and interband magneto-optical transitions in InP," *Phys. Rev. B,* vol. 12, pp. 5803–5810, 1975.

[55] C. G. Van de Walle, "Band lineups and deformation potentials in the model-solid theory," *Phys. Rev. B,* vol. 39, pp. 1871–1883, 1989.

[56] N. Binggeli and A. Baldereschi, "Determination of the hole effective masses in GaAs from acceptor spectra," *Phys. Rev. B,* vol. 43, pp. 14734–14737, 1991.

[57] K. Alavi and R. L. Aggrawal, "Interband magnetoabsorption of $In_{0.53}Ga_{0.47}As$," *Phys. Rev. B,* vol. 21, pp. 1311–1315, 1980.

[58] G. Lehmann and M. Taut, "On the numerical calculation of the density of states and related properties," *Phys. Stat. Sol. (b),* vol. 54, pp. 469–477, 1972.

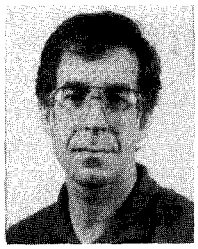

David A. Ackerman was born in Passaic, NJ, in 1954. He received the A.B. degree with honors from Cornell University, Ithaca, NY, in 1976 and the M.S. and Ph.D. degrees in physics from the University of Illinois, Urbana-Champaign in 1978 and 1982, respectively.

In 1983, he jointed AT&T Bell Laboratories, Murrary Hill, NJ. From 1983 to 1991, he worked on the design and development of semiconductor lasers for telcommunications, including devices for submarine cable, high-speed terrestrial and analog systems. He also worked on fabrication of compact narrow-linewidth sources and methods for advanced lightwave packaging. In 1992, he joined the research area at Bell Labs where he is currently working on semiconductor laser measurement, characterization, and modeling.

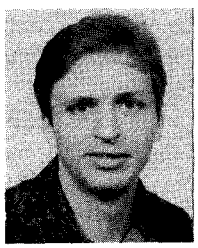

Gleb Shtengel was born in Novosibirsk, Russia, in 1968. He received M.Sc. degree with honors from St. Petersburg State Technical University in 1991.

In 1991, he joined the semiconductor quantum electronics laboratory at A. F. Ioffe Physical-Technical Institute. He studied fast dynamics and high-frequency modulation of semiconductor lasers. In 1993, he was a visiting scientist at Colorado State University, where he worked with vertical cavity surface emitting lasers. Currently Gleb Shtengel is with AT&T Bell Laboratories. His research interests are physical and optical properties of semiconductor lasers, laser dynamics and semiconductor laser based systems.

Mr. Shtengel is a member of LEOS.

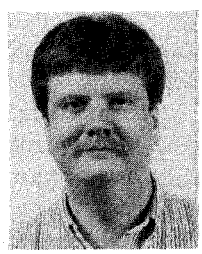

Mark S. Hybertsen was born in Portland, OR in 1958. He received the B.A. degree in physics from Reed College in 1980 and the Ph.D. degree in physics from The University of California, Berkeley in 1986. His thesis research concerned exchange and correlation in semiconductors and insulators.

He joined AT&T Bell Laboratories as a post-doctoral member of technical staff in 1986. He has been a member of technical staff since 1988, conducting a variety of research projects on the electronic properties of materials. His research in the past two years has focused on laser modeling.

Dr. Hybertsen is a member of the American Physical Society and the Optical Society of America.

Paul A. Morton (M'87) was born in England in 1962. He received the B.Sc. and M.Eng. degrees in electronic engineering from the University of Bath, England, in 1984 and 1985, respectively.

He worked on novel optical logic devices and fiber optic signal processing systems. He joined Marconi Defence Systems Ltd. and worked on the dynamics of semiconductor laser diodes at the G.E.C. Research Center and the University of Bath, receiving the Ph.D. degree in 1988. He joined the University of California at Santa Barbara in October 1988 as a post-doctoral researcher, where he worked on active mode-locking of semiconductor lasers using novel devices and cavity geometries, together with device modeling. In January 1991, he joined the Semiconductor Electronics Research Department at AT&T Bell Laboratories, Murray Hill, NJ, where he works on high performance optoelectronic sources. Current interests include high speed lasers and integrated laser/modulators, mode-locked optical pulse sources using fiber grating cavities, and understanding the physics of temperature effects in long wavelength lasers.

Dr. Morton is a senior member of the IEEE Lasers and Electro-Optics Society.

Rudolf F. Kazarinov was born in Russia in 1933. He received the M.S. degree in physics from the Leningrad Polytechnical Institute, Leningrad, Russia, in 1958, and the Ph.D. degree in physics from the Ioffe Institute of Technical Physics, Leningrad, in 1962.

From 1958 to 1977, he worked for the Ioffe Institute of Technical Physics. His research interest was in the physics of semiconductors and semiconductor devices. He was first concerned with semiconductor lasers in 1963, when he applied for the original patent of double heterostructure lasers (with Zh. I. Alferov) in March, 1963. In 1979, he joined AT&T Bell Laboratories, Murray Hill, NJ. His research interests are primarily semiconductor lasers and integrated optics.

T. Tanbun-Ek, photograph and biography not available at the time of publication.

R. A. Logan, photograph and biography not available at the time of publication.